

FULL PAPER

Combined CFA-AFM precipitation interaction-analytical approach for individual and multiple monolayer crystal growth production based on surface area measurements with model surface roughness analysis (Irregularly-shaped surfaces)

Nagham Shakir Turkie | Sarah Faris Hameed*

Department of Chemistry, College of Science,
University of Baghdad, Baghdad, Iraq

The objective of this research was to connect FIA using developed instrument NAG-4SX3-3D analyzer with AFM to explain the surface morphology. Based on the reaction of Fe (II) ion with $[\text{Fe}(\text{CN})_6]^{3-}$, in order to form a blue precipitate, a steady feed was used to achieve an appropriate amount of weight for the AFM study. In relation to the type of precipitate formed, different factors of AFM photograph surface roughness analysis were referenced to clarify the study of surface topography: Skewness, Kurtosis, peak-peak, ten peak height, wave length, fractal dimension, reduced valley depth and core roughness depth, all of which, primarily dealt with the four parameters hybrid, spatial, amplitude and functional. Since no prior study of such has been conducted, all common modes of imaging have been discussed, i.e., contact, non-contact and Occasional contact was defined. In this work, a non-contact mode was used. A comprehensive investigation was done about how the first mono layer is built up by crystallization process and also, how much each grain represent a concentration with the number on the first mono layer. The number of surface area calculation samples was given plus a demonstration of the multi monolayer hypothetically formed especially at high reactant concentration. The primary purpose of the project was to connect AFM to FIA, which is seen as a modern method that could be a very valuable interpretation for other researchers. This gives this research a novelty as no previous study has addressed it. As most FIA method emphasis on the method by developing any methodology for determination of ionic species without regarding the surface morphology of the precipitated molecular ion followed by the formation of nuclei, small particulate then finally forms granules which was studied by SPM.

***Corresponding Author:**

Sarah Faris Hameed

Email: sarahf.hameed@yahoo.com

Tel.: +07706234541

KEYWORDS

Atomic force microscopy; scanning probe microscope; flow injection analysis; mode of operation Fe(II).

Introduction

AFM is one of the newest techniques for the characterization of surface morphology. The information provided by AFM does not duplicate that of SEM but is generally quite

complementary. SEM photos can be used to study surface features that are several tenths of a nanometer while the resolution of AFM is less than 0.1 nm. Therefore, AFM has the ability to distinguish objects on smooth surfaces of molecular dimensions.

Atomic force microscopy (AFM) is used for quantitative and qualitative data based on different properties like morphology, size, surface roughness, and texture [1]. It is used for the 3D characterization of NPs as compare with other techniques like electron microscopy, dynamic light scattering, and optical characterization methods. It also provides details about the different geometries of NPs, an analysis of hydrated NPs, and physical properties like magnetic behavior. It is also used for the study of soft and hard synthetic materials regardless of their conductivity and opaqueness [2]. In AFM, the force between the sharp probe tip (<10 nm) and the sample surface, with a 0.2–10 nm probe-sample separation, is measured [3]. The probe is attached with a cantilever, which deflects upon interaction; this deflection is measured by the reflection of a laser beam by the “beam bounce” method. Therefore, the topography of the surface is directly measured by the deflections of the cantilever. The topography map takes the form of different

peaks which are represented by different color gradients (red, orange, yellow, etc.) or grayscale. In this way, a multicolor sample surface topology image is produced which can be very helpful for the identification and measurement of parameters under investigation.

Figure 1 shows the principle of Atomic Force Microscope. The AFM measures the forces acting between a fine tip and a sample. The tip is attached to the free end of a cantilever and is brought very close to a surface. Attractive or repulsive forces resulting from interactions between the tip and the surface will cause a positive or negative bending of the cantilever. The bending is detected by means of a laser beam, which is reflected from the backside of the cantilever [4,5]. As far as a component of AFM is concerned, Piezoelectric property is used to induce different modes of action that will be dealt with in the next coming paragraphs. Figure 1 shows the main components.

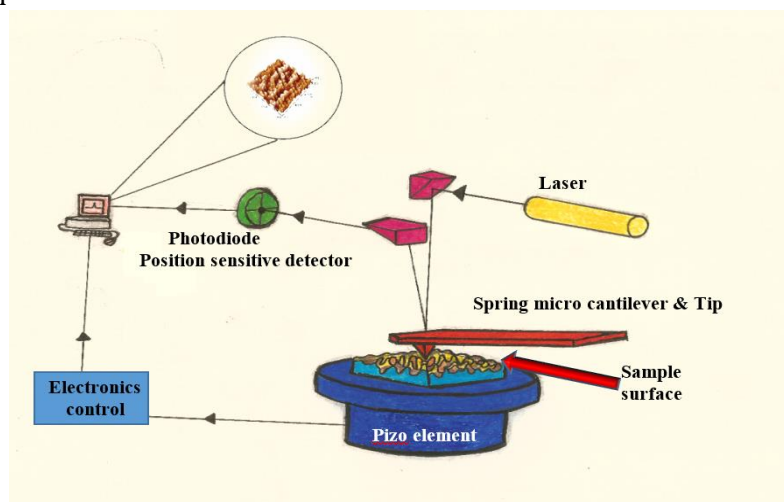


FIGURE 1 AFM components

A probe is made of silicon nitride attached to a cantilever that oscillate on the sample surface during scanning of surface topography, while the sample is placed on a stage that is part of the tool (AFM) on the back of the cantilever of a mirror that reflects the laser beam that is directed and reflect its light to a chart paper x-y recorder with z- axis to measure both x-y for surface parameter and z

for depth that explains a lots of details and is quite important parameter.

The cantilever moves in the form of raster bases always starting in the same way that one can draw by using a ruler. Figure 2 shows the attraction – repulsion forces induced during the work of plotting the topography for precipitate surface [6-8].

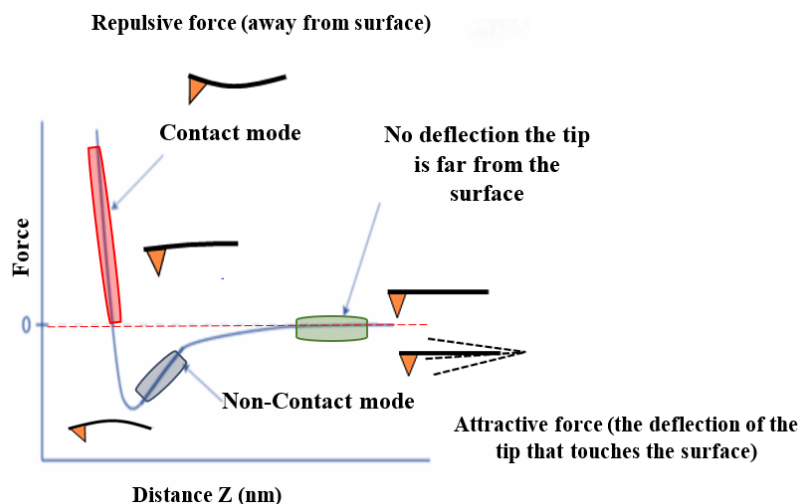
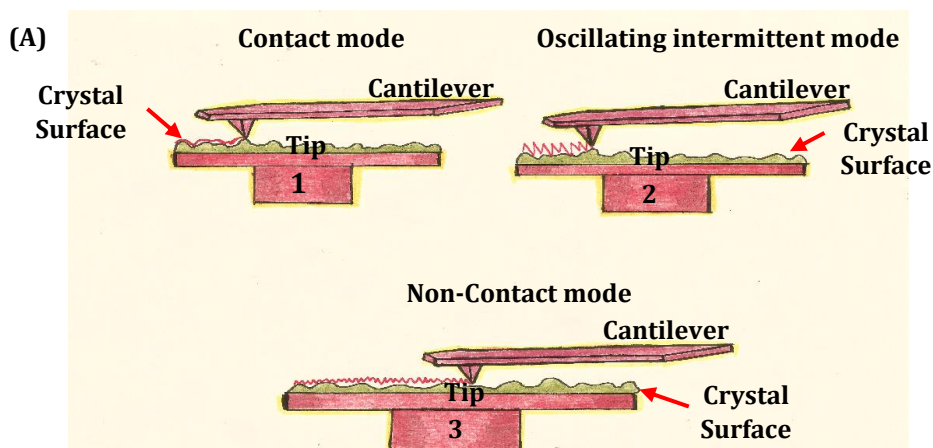


FIGURE 2 Force Graph Curve & tip – sample separation

Mode of operation: Briefly, three modes of operation are common in using the AFM instrument for scanning of contour of precipitated surface. Figure 3A & B shows a representation working of these three modes [9,10]:

- 1) Contact mode when the probe tip touches the sample surface,
- 2) Non- contact when the tip of the probe does not really touch the surface, and
- 3) Oscillating intermittent mode when the tip oscillates above the sample.



1. feedback: deflection level
The cantilever base height is modified by the feedback mechanism to maintain the deflection steady as the tip passes across the surface (friction force microscopy, AFMM conductive probe).

2. feedback: Amplitude of oscillation. The cantilever oscillates and the tip, at the lowest point of the oscillation, makes repulsive contact with the sample surface (tapping mode AFM)

3. feedback: Amplitude of oscillation. The cantilever oscillates near the sample surface without any contact with the electro static/ magnetic force microscopy of the surface .

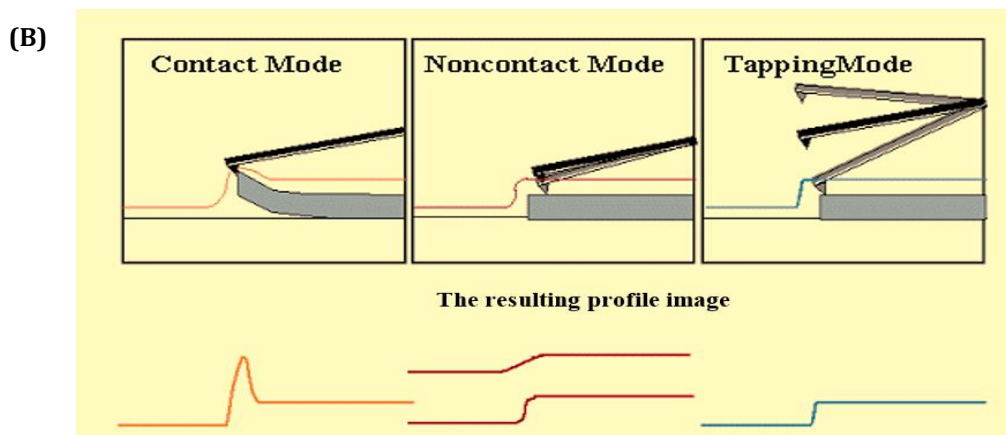


FIGURE 3 A) AFM can be used in a variety of ways, including contact, noncontact, and tapping modes. B) The result profile photograph and the versus mode of operation

The choice of these three modes will be in use for certain types of sample, e.g., soft tissue where there is a great need not to destroy the sample. Semiconductor usually solid. Contact mode will be in use, while in the case that will be presented in their work non-contact mode was used. In contact mode the tip may get enlarged due to friction with the sample surface or cause sudden rise which might help in having misestimation of the results. As sudden repulsion of the cantilever followed by the rise above the real set.

In this work, a novel approach is presented with regard to the relationship between atomic force microscopy with continuous flow injection analysis and how to study different kind of surfaces that might be obtained during various steps in precipitation reaction for determination of ferrous (II) ion drug, as the precipitate was collected during the study of calibration graph using NAG-4SX3-3D Analyzer and the extension of the use with flow injection [11].

This paper not only discusses AFM and the use of FIA. Which is the first time that is dealt with the comprehensive detailed hypothetical calculation.

Experimental

Chemicals

Analytical-reagent quality compounds were both used while distilled water was used to

prepare the solutions. A stock solution of Fe (II) (250 mmol.L⁻¹) was prepared by dissolving Ammonium iron (II) sulfate) NH₄)₂Fe (SO₄)₂.6H₂O, M.wt. 392.14 g mol⁻¹, (24.5088) g in 250 mL, Distilled water and adding 10 mL of sulphuric acid. A Stock solution Potassium ferricyanide, (250 mmol.L⁻¹) K₃Fe (CN)₆, (329.26 g/mol) was prepared by dissolving 41.1575 g in 500 mL of D.W.

Apparatus

The flow instrument consist of four parts as shown in Figure 4, Peristaltic pump-4 channels an Ismatic type ISM 796 (Switzerland), A (Teflon - chem inert) rotary 6-port injection valve, (IDEX corporation, USA), Electronic measuring and readout system, NAG-4SX3-3D [11].

Methodology

The study of AFM start with the preparation of precipitate formed by the reaction of Fe(II) with ferricyanide and collections of samples for study . Sampling is quite important as it reflects the main idea of the kind of precipitate is formed. The collection of precipitate is done during the running of the scatter plot from which the calibration graphs are created, releasing precipitate with different grain property due to variable concentration which indeed represent the whole properties of the precipitate formed.

Low concentration, medium concentration and high concentration reflect the different stages of precipitate formation and crystal growth—depending on the nature of the

precipitate formed. The precipitate is washed with distilled water to remove excess of the reagent used to complete the reaction to form the precipitate of analyte.

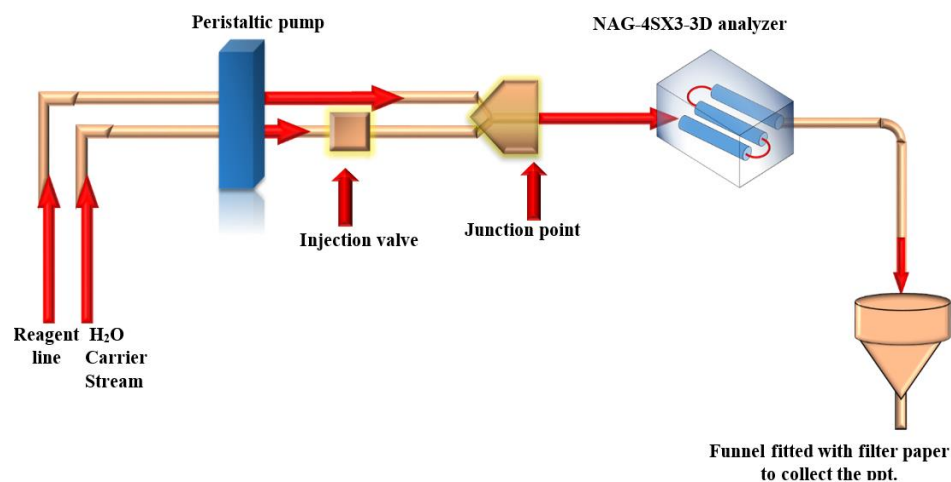


FIGURE 4 Flow injection manifold to measure the reaction product of selected reactant to form a precipitate followed by on-Line filtering the reaction product waste product

A carrier stream line is injected with the sample. A simplified diagram used in this analysis shows the solution that is driven by the movement of a peristaltic pump of a known flow rate (mL/min) to a multiple device Figure, before the reaction product enters the measurement of the formed reaction product where a signal is weakened from the source of incident irradiation.

The response obtained is reported through the x-t potentiometric recorder or any available device for reading. In this research, numerous separate prototypes were proprietary, several variables were presented to contribute to a fine conclusion and all outcomes were examined in a consolidated aspect.

Sampling: A set of precipitate is produced from reactant Fe(II) ion with potassium ferricyanide during the subsequent reaction product as shown in Figure 1.

The sampling is performed in two directions that must be observed.

First: an arbitrary reactant concentration is used before an adequate volume of precipitate is produced on the filter paper

inserted in the funnel to isolate the solution from the precipitate. This collection will provide us with a steady homogeneous precipitate feed.

Second: Using the same set-up, except during scatter plotted calibration graph build up, the precipitate is gathered. This should be considered as random sample so, low (at least replicated for $n=3$ measurement) as well as medium and high concentrations would be obtained. It also requires variable structural formation, but in the end, it comprises just a few milligrams of the same precipitate which are enough for all the analysis to be carried out.

In both cases, extra reagent and other mother liquid chemical used for sampling washing of formed precipitate on the funnel are washed from the funnel. To avoid any grit, the filter paper is left softly sealed overnight after it is dried. For atomic force microscopy contour screening, the sample is ready. AFM did not evaluate the reactant of the expected reaction because of the separate population and cannot be correlated with the precipitate as fineness, i.e. the grain size would be entirely

different from the precipitate obtained because of the development policy.

Figure 5 shows the impact of tip-sample contact on the scanned surface of the shaped precipitate.

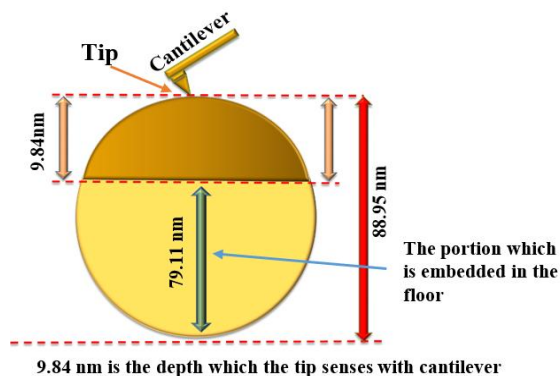


FIGURE 5 A comparison between the probe scan and the apparent height of the granules

The Granularity cumulation distribution report was supplied by AFM. Given Grain number, average diameter, and variance percentage of 50%, 10% and 90% of a variable diameter. Here the assumption is a sphere as diameter applies only for Circles and Spheres. Also, a table of diameter of Grain vs. % of availability is expressed at e (%) that is the current passing through the sample stage during scanning.

TABLE 1 Distribution of Granularity Cumulation reveals

Grain No.:156	<=10% Diameter:55.00 nm
Avg. Diameter:88.95 nm	<=90% Diameter:115.00 nm
<=50% Diameter:80.00 nm	

Diameter(nm)<	Volume(%)	Diameter(nm)<	Volume(%)	Diameter(nm)<	Volume(%)
55.00	1.28	90.00	6.41	125.00	2.56
60.00	8.97	95.00	8.33	135.00	1.92
65.00	4.49	100.00	8.97	145.00	0.64
70.00	5.77	105.00	4.49	150.00	1.92
75.00	8.97	110.00	4.49	155.00	1.28
80.00	7.69	115.00	3.21	175.00	0.64
85.00	13.46	120.00	4.49		

A histogram plot is also given for the distribution of grain diameter. A mathematical treatment of data using data smoothing and Savitzky-Golay via second. vs curve fit (usually 35%, sometimes more, is required and might reach 75% to get the direction of crystal growth whether going to large particle formation or too small particle formation or it is of Gaussian distribution [12-14].

Result and discussion

This study discusses the AFM concept in both the description of surface morphology and surface growth. Table 1 and Figure 6 (A&B) illustrate Grain No. 156 and Avg. Diameter 88.95 nm. The collected data of diameter versus volume and granularity cumulation distribution are summarized in Table 2. Figure 7. pertains to the study of the image surface roughness analysis for the reaction between Fe(II) with $[Fe(CN)_6]^{3-}$; the obtained data are summed up in Table 2 while Figure 7 (A & B) shows Variation of % volume versus granules & data smoothing using Savitzky-Golay. Figure 8 and Table 3 sum up the granularity cumulating distribution in three-dimensional shapes, demonstrating difference in volume supply with granule diameter and number of grains.

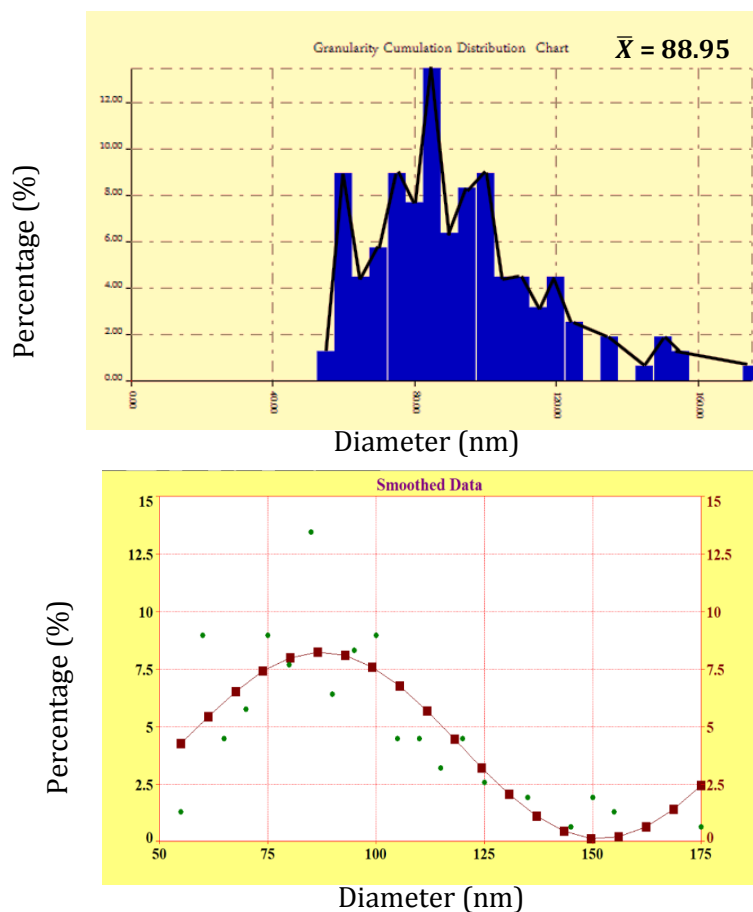


FIGURE 6 A) Distribution of Granularity Cumulation reveals charts. B) Smooth data Gaussian of distribution of Granularity

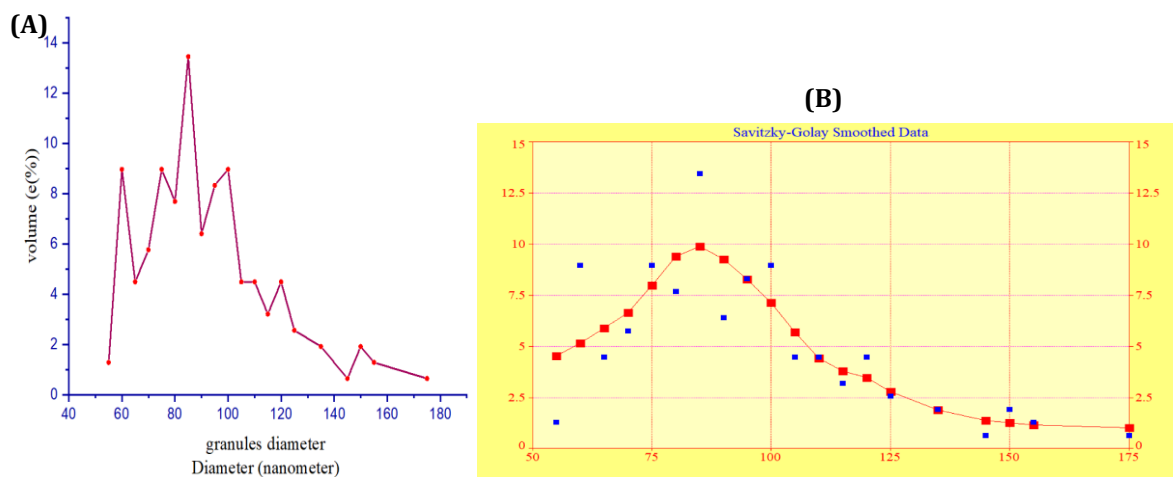


FIGURE 7 A) Variation of % volume versus granules. B) Savitzky -Colay Smoothed data

TABLE 2 Distribution cumulative report of formed granules diameter

Diameter nanometer	Volume e(%)
55	1.28
60	8.97
65	4.49
70	5.77
75	8.97
80	7.69
85	13.46
90	6.41
95	8.33
100	8.97
105	4.49
110	4.49
115	3.21
120	4.49
125	2.56
135	1.92
145	0.64
150	1.92
155	1.28
175	0.64

TABLE 3 Cumulative report on formed granules, including diameter and number of grains

Diameter nm	Volume e(%)	no. of grain
55	1.28	2
60	8.97	14
65	4.49	7
70	5.77	9
75	8.97	14
80	7.69	12
85	13.46	21
90	6.41	10
95	8.33	13
100	8.97	14
105	4.49	7
110	4.49	7
115	3.21	5
120	4.49	7
125	2.56	4
135	1.92	3
145	0.64	1
150	1.92	3
155	1.28	2
175	0.64	1

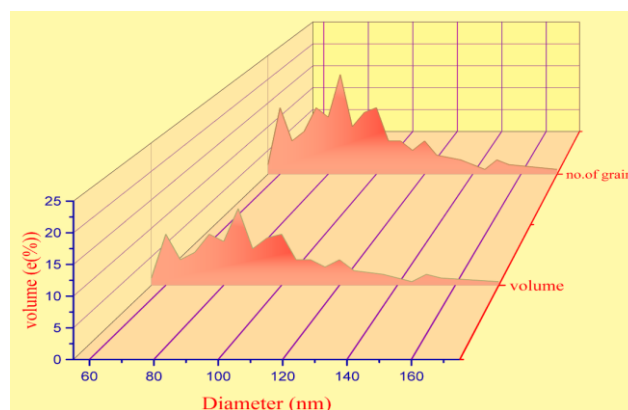


FIGURE 8 Granularity cumulating distribution in three-dimensional shapes, demonstrating difference in volume supply with granule diameter and number of grains

Four parameters will be dealt with given by AFM instrument. The most important items in each parameter is dealt with as follows.

❖ *Amplitude parameter*

- Roughness average= 1.94 nm → suggests a shift toward small size crystals, while the depth is 9.84 nm of the system above (i.e., the reaction between Fe(II) with $[\text{Fe}(\text{CN})_6]^{3-}$);
- (surface skewness) = -0.146 indicates a push toward formation of large diameter granules. Full symmetry is lacking here as 0.00 is a full symmetry, i.e., the same kind of crystal of high purity while -0.146 is the movement toward value of large granules or the presence of impurities of larger diameter than the pure form of grains. This is proved by the surface kurtosis of 2.34 which is within the region of platykurtic toward kurtosis < 3 i.e., distribution of granules and tails are wider than the normal distribution. Platykurtic means that there is a good deal of outlier values (speed of growth and its accumulation causes different size of particulate). This necessitate that if the precipitate should be used as for example a new drug, further purification is necessary.

In addition to the value of 2.34 for surface kurtosis, there is a large sum of impurities which might be a very helpful in semiconductor industry while in drug preparation with a high purity compound, a further purification is required. This depends on

active ingredient forming the main drug used, i.e. the potency and dose, which suggest small soft gel like granules that are overcrowded causing press of layer, or what is called first or even second and so on larger unseen by the probe because of its pressed layer of granules. Surface skewness of -0.146 suggests a push to the formation of large agglomerates of gel soft particulate forming large bulky granules. No full summary is shown in the SPM, which is a clear indication of the function of random agglomerates causing unclear symmetrical profile; symmetrical profile will have skewness value of 0.00, i.e., all particulate formed or even any impurities will have the same dimension, i.e., regular buildup of final granules that will characterize the resulted reaction product with any if an added certain species that will help in building the resultant granules to certain frequency or wavelength with impurity with electron from the probe tip. Reaction sample collection is preferred due to the formation of variation dimension of granules depending on concentration used while constant concentration is used for feeding. There will be specificity in preferring a pre determination mode of granule formation. The root mean square of 0.191 is equivalent to angle of $23.607 \sim 23.61^\circ$. Low slope indicates no strong buildup of granules is formed as this value shows the closeness to the x-axis, i.e., $t_{\text{sec}(\text{dmm})}$ axis a good spreading value. For this kind of particulate formed,

higher slope value will indicate a crystalline irregular shape that causes $Y_{z(mv)}$ to be high.

❖ Seemingly, short distance of peak-peak (10.4 nm) will not allow buildup of a large granules. Therefore, it is not able to grow up

on the larger size or higher peak, i.e.; granules when drawn by the effect of probe, this shown by Ten point height: $5.52 \text{ nm}/5=1.104 \text{ nm}$ (height for each grain), as shown in Figure 9.

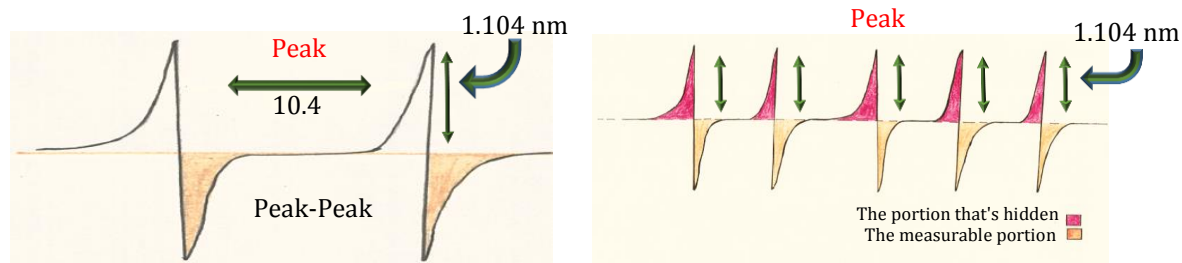


FIGURE 9 The peak to peak and ten-point height parameters obtained from AFM data

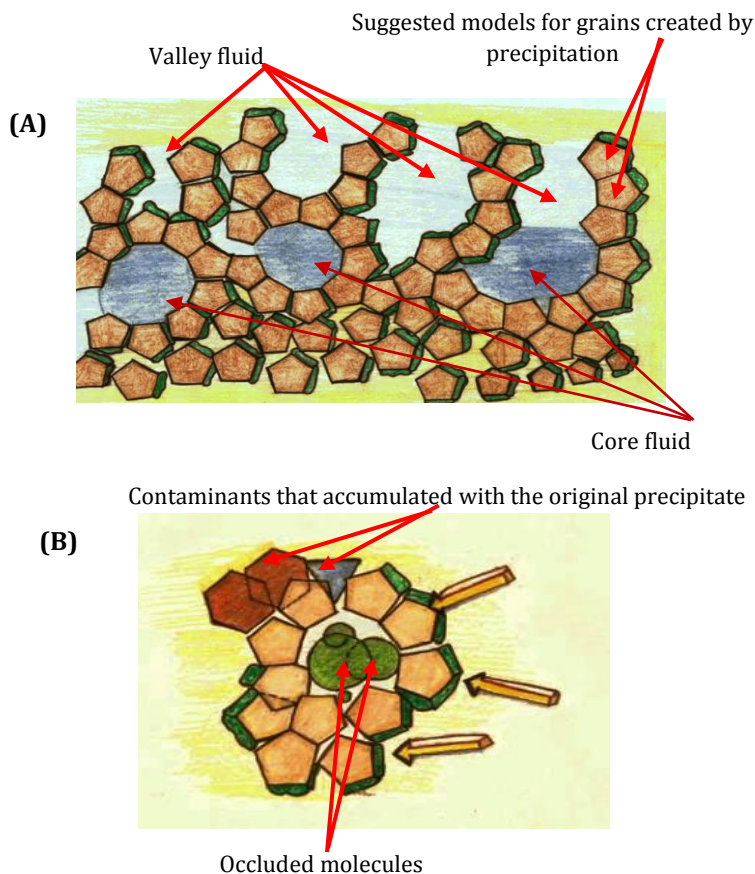
❖ *Factional parameters*

Fractal parameters: -core fluid retention index is 1.47 while valley fluid retention index is 0.115: $\frac{1.47}{0.115} = 12.78 \approx 13$ times

There is water ≈ 13 times in the core relative to what is available at the valley, indicating a rapid growth of nuclei followed by crystal

growth that will trap the water at core leaving the outer surface as a valley that contains 13 times less water. It is expected due to the surface exposure to atmospheric variation of air and warmth.

Surface bearing index=2 explains that there is extra layer of granules as shown in Figure 8 and 10 A, B & C.



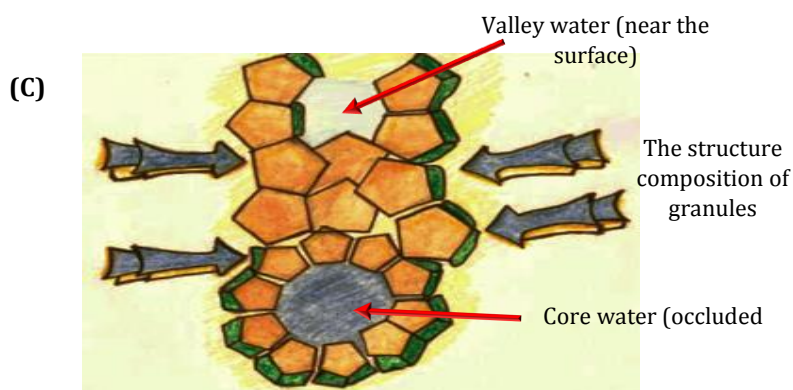


FIGURE 10 A) A hypothetical shape that depicts how the valley and core of a developed precipitate, B) Contaminants trapped in the initial deposition's bottom layer, C) granules' inner structure

❖ *Hybrid parameters:*

With root mean square slope=0.191, the low value of slope indicates grain height is low.

❖ *Spatial parameters:*

It is represented by density of summits=zero [$1/\mu\text{m}^2$]. Zero value indicates that at $1\mu\text{m} \times 1\mu\text{m}$ area, there are no available granules; compared with other precipitate formation that might give a positive value. More than zero value suggests availability of granules at the scanned area (i.e., $1\mu\text{m} \times 1\mu\text{m} = 1/\mu\text{m}^2$).

❖ *Fractal dimension:*

2.36 indicates the scanned fractions of total scanned area dimensions. Pixels=412,416 indicates the number of lightening spots.

So, regarding a pixel simple definition, in digital imaging a pixel or picture element is a physical point in a raster image, or the smallest addressable element in an all points addressable display device, so it is the smallest controllable element of a picture represented on the screen, as shown in Figure 11. So, Figure 12A & B shows the image surface roughness analysis of precipitate formed in Flow Injection Analysis via Atomic force microscopy and the results are summed up in Table 4.

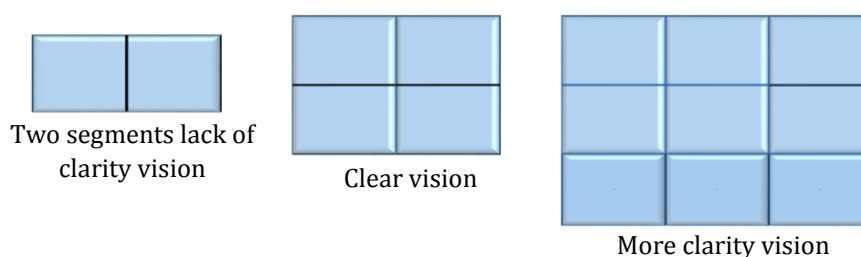


FIGURE 11 Pixel clarification

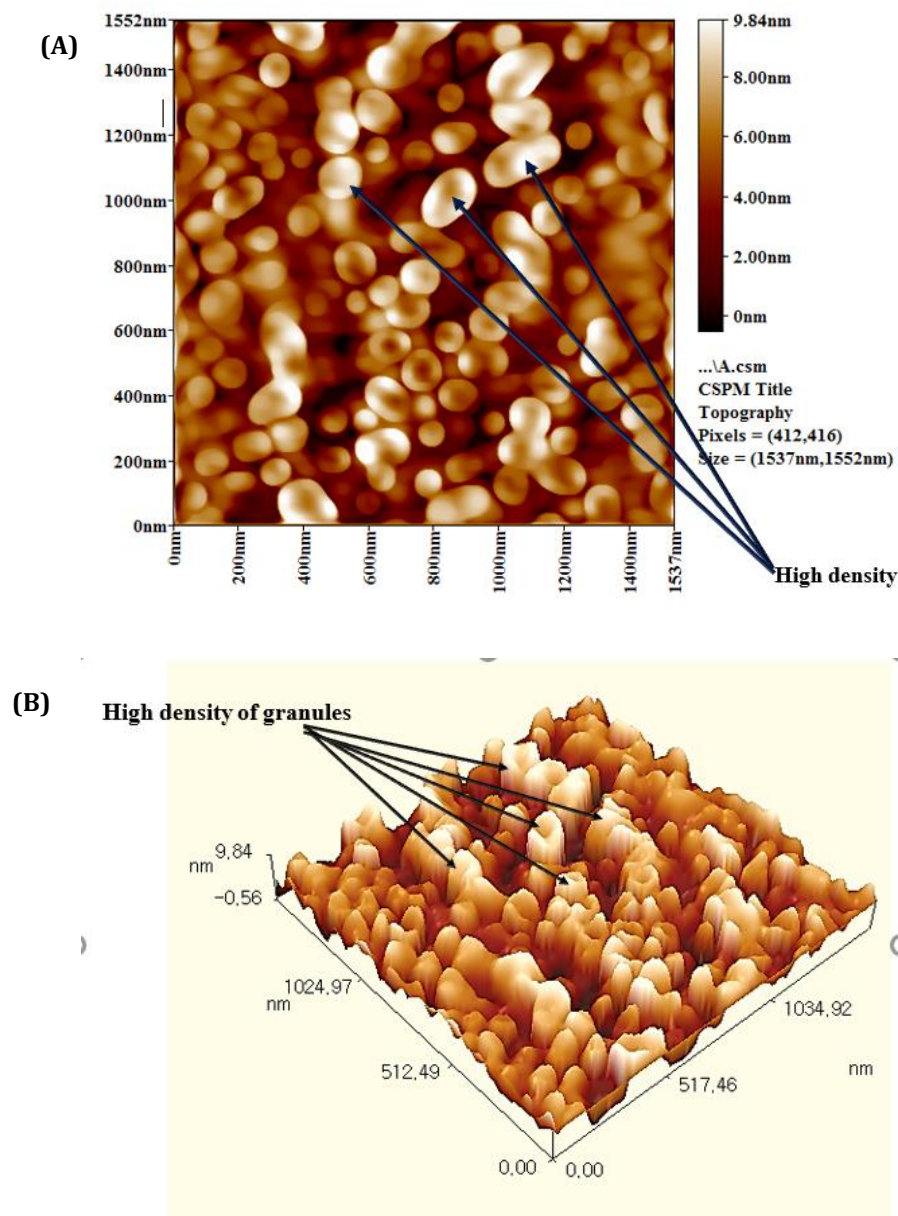


FIGURE 12 A) The scale and density of the precipitates was shown by AFM micrographs. B) Analysis by AFM topographical describing the depth of surface roughness by (3D) three-dimensional diagram of the reaction Fe (II) Ion with $[\text{Fe}(\text{CN})_6]^{3-}$ to form blue precipitate.

TABLE 4 Portrait roughness study of the surface by AFM

The Parameters of amplitude		Value
Sa(Roughness Average)		1.94 nm
SsK(Surface Skewness)		-0.146 nm
Sku(Surface Kurtosis)		2.34
Sy(Peak-Peak)		10.4 nm
Sr(Ten Point Height)		5.52 nm
Hybrid Parameters		
Ssc(Mean Summit Curvature)		-1 [1/nm]
Sdq(Root Mean Square Slope)		0.191[1/nm]
Sdr(Surface Area Ratio)		2
Factional Parameters		
Sci(Core Fluid Retention Index)		1.47
Svi(Valley Fluid Retention Index)		0.115
SpK(Reduced Summit Height)		1.28 nm

Sk(Core Roughness Depth)	6.37 nm
Svk(Reduced Valley Depth)	2.17 nm
(Depth)	9.84 nm
Grain no.	156
Average Diameter	88.95 nm
Spatial Parameters	
Sds(Density of Summits)	0[1/μm ²]
Fractal Dimension	2.36
Pixels	412,416
Scanned Area	1537 nmX1552 nm

As follows, the calculation that deals with surface contour by AFM estimation:

1- Surface area of scanned section Figure12. = 1537 nm x1552 nm → surface area = 2385424 nm²

2- Surface area of single granules= $4\pi r^2 \rightarrow 4 \times 3.14 \times \left(\frac{88.95}{2}\right)^2 = 24844.00185 \text{ nm}^2$.

3- Total surface area of all granules= 156 x 24844.00185 nm² = 3875664.289 nm².

4- Remained area as a second of first ground monolayer i.e., extra area remained:-

2385424 nm² - 3875664.289 nm² = - 1490240.28 nm².

This means the area of second of first ground monolayer

5- So, the number of granules in the above ground monolayer calculated by being divided with the surface area of single sphere is as follows:

$-1490240.28 \text{ nm}^2 / 24844.00185 \text{ nm}^2 \rightarrow 59.9839 \approx 60$ granules extra

This number of granules means the extra area above the first ground monolayer.

6- So, the number of grains in the first ground monolayer is:

156 - 59.984=96.016093 grains

Or surface area of ground monolayer / surface area of single granules is:-

$2385424 \text{ nm}^2 / 24844.00185 \text{ nm}^2 = 96.016093$ granules

7- The area that each granule will occupy in the first ground monolayer is:-

$2385424 \div 96.016093 \text{ grains} \rightarrow 24844.00193 \text{ nm}^2$ occupied surface area by 96 grains and the surface area occupied by each granule in the second monolayer

1490240.28 nm²/59.9839 grains → 24844.00185 nm² occupied surface area by 60 grains.

Note: - The negative sign will be neglected.

So, first ground monolayer → 2385424 nm² (≈96 granules)

Second monolayer → 1490240.28 nm² (≈60 granules)

8- The concentration in the first ground monolayer based on Avogadro's no. = 6.02×10^{23} can be found as follows: -

$\frac{96.016093 \text{ granules}}{6.02} \times 10^{-23} \times 1 \text{ mol/L} \rightarrow 1.59495 \times 10^{-22} \text{ mol/L}$

In the second monolayer (extra area or side walk), the concentration is: -

$\frac{59.9839}{6.02} \times 10^{-23} \times 1 \text{ mol/L} \rightarrow 0.9964103 \times 10^{-22}$

The concentration of each single granule is:

$\frac{1.59495 \times 10^{-22}}{96} = 1.66 \times 10^{-24} \text{ mol}$

no difference here

$\frac{0.9964103 \times 10^{-22}}{60} = 1.66 \times 10^{-24} \text{ mol}$

Table 3 shows the number of grains for the reaction of Fe(II) with [Fe(CN)₆]³⁻ based on volume e(%) and number of granules (156) .So, there are 20 variables of a volume % of granules of different diameter. It is possible that to find out the number of each diameter upon the % a availability - Based on the given availability we have:

<=10% diameter: 55 nm = 15.6 grains

<=50% diameter: 80 nm = 78 grains

<=90% diameter: 115 nm = 140.4 grains

The combination of 15.6+78+140.4=234 of 150 % are equivalent to 156 at 100%.

- At low supersaturation, particles can grow faster than they nucleate, due to a greater crystals grain size because the rate growth should be proportional to the square of supersaturation, while at high supersaturation, crystal nucleation dominates crystal formation, eventually resulting in smaller crystals, which is actually due to the growth rate that should be directly proportional to the supersaturation.

The creation of monolayer results from the fields that rise quickly to the boundaries, as shown in Figure 13.

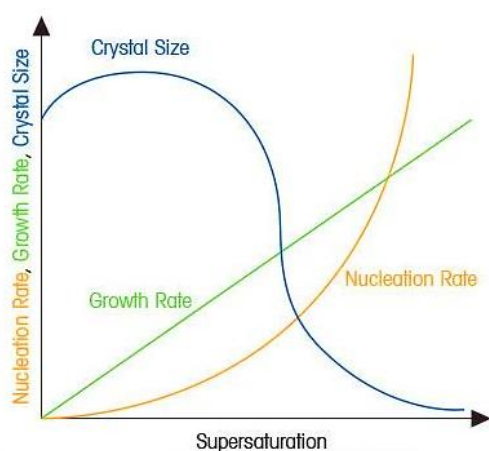


FIGURE 13 The relationship between supersaturation, nucleation, growth, and crystal size demonstrates how crucial it is to monitor supersaturation when making crystals of the desired size and distribution

Conclusion

The combination of CFA with AFM to study the precipitate particles for the reaction of Fe (II) Ion with $[\text{Fe}(\text{CN})_6]^{3-}$ formed a blue precipitate. It was shown that with von weimarn ratio, a Particle size of precipitation is inversely proportion to the relative supersaturation of the solution during the precipitation process". So, we consider the difference in number and size of precipitation grains regarding concentrations of the precipitating reagents Von weimarn relation $\rightarrow \frac{Q-S}{S}$, while Q= total salt concentration, S = Molar solubility, which increases with increasing the temperature.

- If $\frac{Q-S}{S}$ = large number, it refers to formation of large number of granules with small size which lead to this output, contributing significantly to the presence of intermediate spaces and therefore the attenuation of the light is very poor
- If $\frac{Q-S}{S}$ = small number, it refers to the creation of low number of granules with large size $Q/S-1$; the large granules attenuate the light considerably.

The temperature of reaction will increase the solubility, even PH value will be different in various temperatures. Reagent concentration and volume of sample loop will play a significant rule in obtaining a supersaturation at the outlet junction, and even it is not recommended. Teflon tubes have been used since they have the characteristics of hydrophobicity, i.e. they resist water moves.

The working range i.e., linear dynamic range and calibration range can be used and all of these depend on the analyst. When the area of scanned surface by AFM subtracting from the total granules surface area, the results found will be of two choices either positive or negative.

- If the data gained are positive (result of subtraction), it indicates there is still a space for more granules to build up because since concentration of created granules would fill first ground monolayers; this could happen at low reactant concentration only i.e., at lower section of the scatter plot.
- If the data collected (subtraction values) are negative, it simply means there will be no space at the first ground monolayer.

Monolayers cause buildup of new second monolayer. It may happen at the average \bar{X} and \bar{Y} , i.e., the centroid value of the scatter plot of X (analyte concentration) vs the obtained response (Y), which is supposed to correlate with average developed precipitate (formed granules), just at this point based on the availability of excessive additional granules that covers up the second ground

monolayer (or even portion of its surface area).

At the point of $-1490240.289 \text{ nm}^2$ there is no more space in the first ground monolayer to accept additional granules, as represented in Figure 14.

Acknowledgements

We would like to express our heartfelt gratitude to Prof. Issam Mohammad Ali Shakir for his excellent guidance and support in completing this research and providing us with all of the necessary resources.

References

- [1] G. Binnig, C.F. Quate, C. Gerber, *Phys. Rev. Lett.*, **1986**, *56*, 930–933. [[crossref](#)], [[Google Scholar](#)], [[Publisher](#)]
- [2] D.J. Müller, Y.F. Dufrêne, *Trends Cell Biol.*, **2011**, *21*, 461–469. [[crossref](#)], [[Google Scholar](#)], [[Publisher](#)]
- [3] B. Huang, H. Babcock, X. Zhuang, *Cell*, **2010**, *143*, 1047–1058. [[crossref](#)], [[Google Scholar](#)], [[Publisher](#)]
- [4] P. Nguyen-Tri, P. Ghassemi, P. Carriere, S. Nanda, A.A. Assadi, D.D. Nguyen, *Polymers*, **2020**, *12*, 1142. [[crossref](#)], [[Google Scholar](#)], [[Publisher](#)]
- [5] H.J. Butt, B. Cappella, M. Kappl, *Surf. Sci. Rep.*, **2005**, *59*, 1–152. [[crossref](#)], [[Google Scholar](#)], [[Publisher](#)]
- [6] Mr. Sameer, S.S. Gajghate, *Introduction to Atomic Force Microscopy (AFM)*, National Institute of Technology Agartala, **2017**, [[crossref](#)], [[Publisher](#)]
- [7] L. Zang, **2017** (Online). Available at: http://www.eng.utah.edu/~lzung/%0Ahttp://www.eng.utah.edu/~lzung/images/%0Awww.eng.utah.edu/~lzung/images/Lecture_10_AFM.pdf.
- [8] W.C. Sanders, *Atomic Force Microscopy Fundamental Concepts and Laboratory Investigations*, 1st Edition, **2019**, 1-17. [[crossref](#)], [[Google Scholar](#)], [[Publisher](#)]
- [9] Y.F. Dufrêne, T. Ando, R. Garcia, D. Alsteens, D. Martinez-Martin, A. Engel, C. Gerber, D.J. Müller, *Nat. Nanotechnol.*, **2017**, *12*, 295–307. [[crossref](#)], [[Google Scholar](#)], [[Publisher](#)]
- [10] D. Guo, G. Xie, J. Luo, *J. Phys. D. Appl. Phys.*, **2014**, *47*, 013001. [[crossref](#)], [[Google Scholar](#)], [[Publisher](#)]
- [11] IRQ. PATENT. No. 6100, I.M.A. Shakir, N.S.T. Al-Awadie, Novel Multiple Continuous Flow Cells (hydrophilic & hydrophobic) works as a Solo Flow cell with Summed S/N responses in NAG- 4SX3 – 3 D instrument .2020, patent, International classification G01N2021/0325 , Iraqi classification 6 .
- [12] A. Savitzky, M.J.E. Golay, *Anal. Chem.*, **1964**, *36*, 1627–1639. [[crossref](#)], [[Google Scholar](#)], [[Publisher](#)]
- [13] H. Kordestani, C. Zhang, *Sensors*, **2020**, *20*, 1983. [[crossref](#)], [[Google Scholar](#)], [[Publisher](#)]
- [14] J. Luo, K. Ying, J. Bai, *Signal Processing*, **2005**, *85*, 1429–1434. [[crossref](#)], [[Google Scholar](#)], [[Publisher](#)]

How to cite this article: Prof. Nagham Shakir Turkie, Sarah Faris Hameed*. Combined CFA-AFM precipitation interaction-analytical approach for individual and multiple monolayer crystal growth production based on surface area measurements with model surface roughness analysis (Irregularly-shaped surfaces). *Eurasian Chemical Communications*, 2021, 3(10), 678-692.
Link:
http://www.chemcom.com/article_136405.html